Simulation of frictional behavior of Sb nanoparticles on HOPG: Frictional duality and biduality

Ján Brndiar, Robert Turanský, and Ivan Štich*

Center for Computational Materials Science, Institute of Physics, Slovak Academy of Sciences, SK-84511 Bratislava, Slovakia

(Received 14 April 2011; revised manuscript received 1 July 2011; published 30 August 2011)

Antimony nanoparticles deposited under UHV conditions on HOPG are experimentally found to exhibit frictional behavior characterized by the presence of three clearly separated frictional branches featuring double dual behavior of dependence of the frictional force on the contact area. We present extensive density functional simulations, augmented to accommodate van der Waals interactions, in order to shed light on the dual frictional behavior. The simulations include incommensurable interface, wide range of spacer molecules and clusters, such as H_2O, O_2, propane, Sb_4 spacer clusters, mobile oxidized nanoasperities as well as multiple friction generators arising from combination of spacer particles. These simulations not only provide deep insights into all the frictional branches experimentally observed but they also provide realistic incarnations of the previous simplified models. In addition, they also yield explanation of experimental results that lie well beyond the scope of the existing theoretical models.

DOI: 10.1103/PhysRevB.84.085449 PACS number(s): 68.35.Af, 62.20.Qp, 73.22.−f

I. INTRODUCTION

Friction at the macroscale is fairly well understood and described by Amonton's law, which states that the friction force $F_f = \mu F_l$ with F_l being the external loading force and μ the friction coefficient. Since μ is constant for a given interface, at the macroscale F_f is independent of the interface contact area A. In addition, Amonton's law implicitly states that the friction force is also independent of sliding velocity. However, tribological properties at the nanoscale change immensely,[1–3] and their understanding is still incomplete. In particular, friction force depends on the contact area A, i.e., $F_f = F_f(A)$,[3,4] and depends also on temperature and sliding velocity.[5,6]

Especially intriguing dependence of frictional force on contact area was observed in recent experiments for antimony nanoparticles sliding on HOPG substrate[7–9] performed under UHV conditions, see Fig. 1. In the first experiment, antimony particles have been prepared under UHV conditions and friction was measured during lateral manipulation. In a second experiment, the particles were exposed to air for several days and subsequently friction was measured inside the UHV system.[7–9] The frictional force dependence on apparent contact area in Fig. 1 indicates presence of a double duality in the frictional behavior characterized by three distinctive, clearly separated frictional branches. The first duality, observed in antimony nanoparticles prepared under UHV conditions, shows either vanishing friction forces or friction forces increasing linearly with the contact area (nonvanishing friction branch). After extensive exposure to ambient conditions the antimony nanoparticles again exhibit a dual friction behavior under UHV conditions; the data points from the same nonvanishing friction branch as in UHV coexist with nanoparticles showing very high friction of roughly an order of magnitude larger.

In order to uncover the double duality in frictional behavior, let us now consider a nanoparticle with a contact area of $\approx 30 \times 10^3 \mathrm{nm}^2$, see Fig. 1. For atomically clean Sb particles on HOPG the friction is ≈3 nN (see the lower branch in Fig. 1), which coexists with a linear high-friction branch yielding 30 nN for the same size particles. After exposing the Sb particles to air, the same 30×10^3 nm^2 Sb particles coexist in a very high-friction state with values reaching 300 nN together with the previously identified nonvanishing friction branch of 30 nN. This cluster size and frictional forces will be used in comparison with our simulations.

The clearly separated frictional branches in Fig. 1 provide an ideal ground for a deeper understanding of the frictional behavior at the nanoscale. There are theoretical models which aim to describe some generic features of the friction at the nanoscale. They are based either on abstract theoretical models or on simulations with simple empirical interactions, such as Lennard-Jones,[10,11] without reference to any realistic system. For example, for incommensurable interfaces, the concept of structural superlubricity applies.[12,13] Hence, vanishing friction is to be expected for most interfaces, which is not observed. Such a discrepancy is explained, even under UHV conditions, by the presence of ubiquitous residual "dirt particles," such as water and hydrocarbons, which will lock the interfaces,[14] leading to linear dependence of the friction force with contact area. These concepts certainly apply also to the antimony nanoparticles on HOPG. The lattice mismatch between antimony and HOPG is about 4%,[15] hence, the structural superlubricity can be expected to be responsible for the vanishing friction branch, whereas the dirt particles may provide explanation for the nonvanishing frictional branch, see Fig. 1.

The most important ingredient of these models is that the spacer particles have to be mobile, as the effect of rigidly bound particles would again lead to incommensurable structures and superlubricity.[11] The importance of mobility of the spacer dirt particles is schematically illustrated in Fig. 2. Due to periodic undulations of the potential energy surface (PES), the effect of immobile spacer particles averages out, whereas the effect of mobile particles may constructively add up and increase the friction force.

The theories also predict scaling relations with contact area. For amorphous interfaces the friction is predicted to scale with the square root of the contact area and for crystalline interfaces even more weakly,[14] whereas for the dirt-particle-mediated friction, linear scaling is predicted.[10,11]

Despite all these generic theoretical considerations, the fact that three distinct clearly separated frictional branches are experimentally observed remains a surprise. Especially

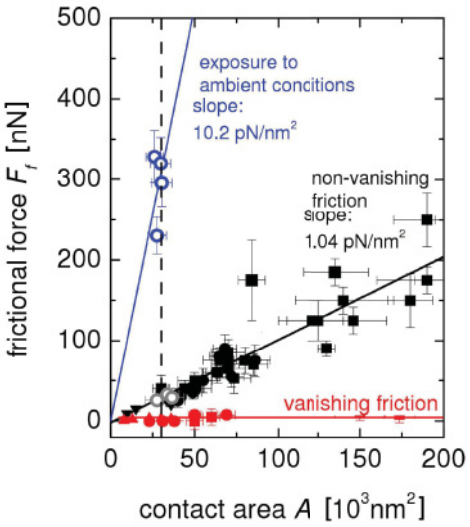

FIG. 1. (Color online) Experimental results for antimony nanoparticles of varying contact area sliding over an HOPG substrate, exhibiting double duality of frictional behavior with three different frictional regimes.[7–9] Data points from nanoparticles prepared under UHV conditions are shown by filled marks, data points after exposure to air are shown by circles. From bottom to top: (a) vanishing friction branch (red/grey points), (b) nonvanishing friction branch (black squares, grey circles), and (c) friction branch corresponding to exposure to air for several days (blue/dark grey circles). The dashed line indicates the position of a 30×10^3 nm^2 particle used as a reference for comparison of experiment and simulation. Adapted from Refs. 7–9.

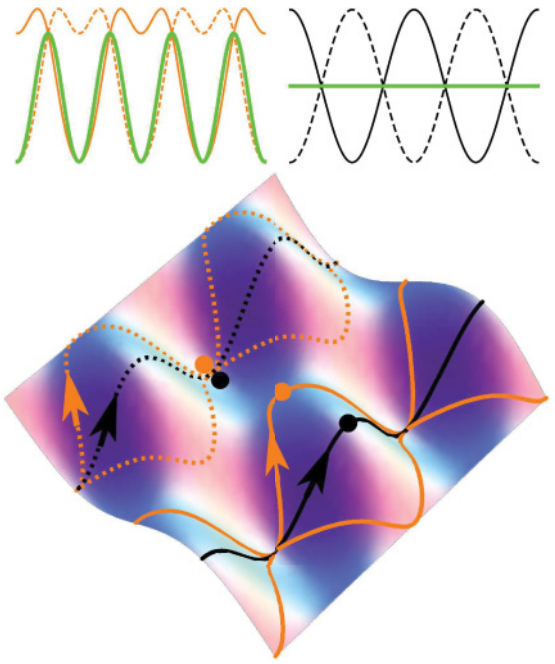

FIG. 2. (Color online) Schematic illustration of the scenarios corresponding to immobile (black lines) and mobile (orange/grey lines) spacers for two particles moving on a model potential energy surface. The upper panels show the respective energy profiles with the average shown in green/grey thick lines.

intricate appears the clear separation between the vanishing and nonvanishing frictional branches. It is not clear why some particles are contaminated by dirt and others are immune. As we explain below, this very clear frictional separation is due, in part, to the fact that the Sb-HOPG is close to an ideal incarnation of a van der Waals (vdW) interface. More reactive interfaces would exhibit more bonding[5] and structural relaxation that might blur the separation.

In addition, while the existing models may provide some insights into the behavior of the Sb-HOPG system under UHV conditions, they provide no insights into the second duality observed for nanoparticles exposed to ambient conditions. Large concentrations of dirt particles may not be compatible with UHV conditions and the observed dual behavior. Models based on the formation of an oxide layer in the Sb-HOPG interface have the problem that such an oxide layer would again result in formation of incommensurable interface and superlubric behavior in stark contradiction with experimental observations. Hence, the high-friction dual branch, Fig. 1, will require presence of other structural ingredients, and we will argue that high-friction mobile oxidized multiasperities provide the required explanation.

The basic paradigm of nanotribological research is that the frictional behavior of a single asperity contact needs to be clarified in order to better understand friction at the nanoscale. Such a realistic insight was provided in our recent short communication.[9] Transcending this preliminary investigation, here we not only present a much more extended and comprehensive account of the simulations but also provide novel data and deeper analyses. In addition, our simulations give access also to quantitative estimates, such as lower dirt particles concentrations/upper bounds of the resulting frictional forces, which make it possible to discriminate between different models. The simulations described below are zero-temperate simulations. Similar simulations could be performed also in dynamical mode at finite temperatures.[16] However, given the size of the nanoparticles experimentally used, tenths to hundredths of thousands nm^2, such dynamical simulations would make little sense. Instead, the friction may be viewed as a sum of individual thermally activated friction-generating processes between two minima (A and B) on the potential energy surface. Hence, a model based on rate constants $k_{A\to B}$ and $k_{B\to A}$ could be constructed[5] with energy barriers needed as input taken from our simulations.

More generally, nanotribology is still essentially based on case studies, with systematics, so important in other fields of physics/chemistry, largely absent. Insights gained from simulations such as those in the present manuscript will play an important role in building the systematics in this field.

II. SIMULATION DETAILS

The simulations are based on density-functional-theory (DFT) modeling within plane-wave pseudopotential formulation using the CPMD[17] simulation package. The exchange-correlation effects were described with rev-Perdew-Burke-Ernzerhof[18,19] exchange-correlation functional. Wave functions were expanded in plane waves at the Γ point of the simulation cell with a 30 Ry cutoff. An ultrasoft pseudopotential[20] was used for carbon, oxygen, and hydrogen

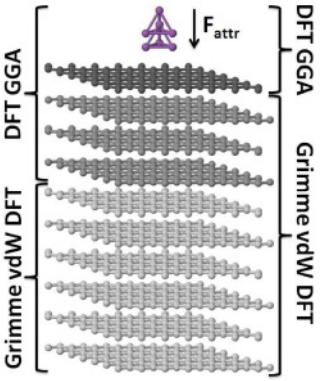

FIG. 3. (Color online) Schematics of the simulation setup illustrated on Sb_4 nanoparticle on HOPG. Two different partitions between "chemically active" and van der Waals regions tested are shown on left and right, with the scheme on the right used in the production simulations.

and a normconserving pseudopotential[21] for antimony. In open-shell systems, spin was explicitly taken into account by performing spin-polarized calculations.[16] Sb-HOPG interface has a strong van der Waals (vdW) bonding and the standard DFT description of the Sb-HOPG interface does not provide the binding of Sb_n to HOPG or the vdW bonding in HOPG itself. The vdW component was fixed by adding Grimme's correction.[22] A schematic simulation setup is shown in Fig. 3. While the vdW component provides most of the "bonding" between antimony and HOPG, it provides very little corrugation of the PES for sliding and hence generates no friction. For example, for the Sb_4-HOPG interface, Fig. 3, the vdW interaction accounts for ∼0.9 eV or ∼0.3 eV/atom, and the short-range chemical interaction accounts for corrugation of the PES of only ∼30 meV, see Fig. 17.

In production simulations, only one graphene layer was included in the "chemical" region. The number of vdW layers were chosen so as to bring the energies and atomic forces to convergence. Inclusion of only one graphene layer in the chemical region compared to three or more layers modified energy profiles by only a few meV with similarly small error in forces. The details of a convergence study are in Appendix along with the tests of the energetics.

In all simulations, an incommensurable Sb-HOPG interface was considered, for details, see Sec. III. We have considered a range of different "dirt particles" associated with imperfect vacuum, which was introduced into the Sb-HOPG interface: oxygen atom and molecule, water, propane, and Sb_4 clusters. In order to test the mobility of the dirt particles and their ability to prevent cancellation of their contributions to friction, we have also considered multiple friction generators of the same kind and their combinations.

All simulations are done at zero temperature by sliding the interface while simultaneously relaxing the atomic positions of all mobile atoms. For simplicity, sliding directions of high symmetry with respect to HOPG were selected and the simulation terminated after mapping out the first period. In most cases, however, we only disclose the part with the dominant energy barrier. From the resulting PES, approximate friction force and/or dirt concentration/friction force estimates are made.

III. INCOMMENSURABLE INTERFACE

The single most important preliminary task to our simulation is the construction of the incommensurable Sb-HOPG interface. As shown below, the lattice mismatch between antimony and HOPG of about 4%[15] invalidates approaches based on models of commensurable interfaces.

Models of incommensurable interface would require infinite unit cells. However, finite-size crystalline approximants to the incommensurable Sb-HOPG interfaces can be constructed. An example of a construction based on a 7×7 HOPG hexagonal cell and an antimony cell cut along [111] plane forming a 4×4 hexagonal slab with the lattice parameter slightly adjusted afterwards so as to form a periodic supercell is shown in Fig. 4. This cell size is sufficient for most simulations. Other approximants to incommensurable interfaces can be generated by choosing different cell sizes and rotations. An example of a larger model of an incommensurable Sb-HOPG interface which we use in part of the simulations below is formed by an HOPG hexagonal cell constructed from the (10,3) elementary cell vector and an antimony cell cut along [111] plane forming a 5×5 hexagonal slab and rotated by 17° again with a slight antimony lattice parameter adjustment to form a periodic supercell.

Simple estimates for the vanishing friction branch can be made from these simulations. Simulation results for the incommensurable structure shown in Fig. 4 yield a friction value of $F = \frac{\Delta E[\mathrm{meV}]}{\Delta l[\mathrm{Å}]} \approx \frac{0.8}{2.5} = 0.32 \frac{\mathrm{meV}}{\mathrm{Å}} = 0.32 \times 1.602\ \mathrm{pN} = 0.5\ \mathrm{pN}$ for the considered area size of 2.6 nm^2. For amorphous interfaces, friction has been shown to scale with the square root of A and for crystalline interfaces even weaker.[14] Hence, for the considered nanoparticle size of 30×10^3 nm^2 we obtain from

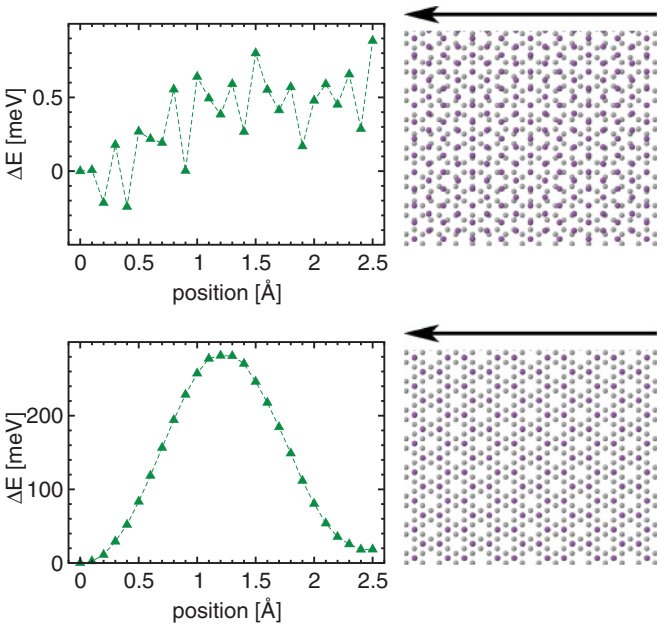

FIG. 4. (Color online) Comparison of incommensurable (upper panel) and commensurable (lower panel) Sb-HOPG interfaces. Shown in each panel are structural models (antimony in violet/dark grey, carbon in grey) and variation of energy during sliding of the interface. The upper arrows indicate the sliding direction of the interface.

our simulation ≈5.8 nN assuming linear scaling or ≈0.05 nN assuming square root scaling. We note that despite the fact that the calculated energies of the order of 0.5 meV are at the limit of the numerical accuracy, the estimated forces are reasonably close to the experimental value of ≈3 nN.

The results for incommensurable structure are in stark contrast to those for the related commensurable interface model, see Fig. 4. Here, assuming linear scaling, we obtain for the 30×10^3 nm^2 particle a friction force of ≈6500 nN. This value, being a factor 10^3 to 10^4 too large compared to the friction forces obtained from incommensurable interface models as well as from the experiment, invalidates the commensurable model.

IV. SPACER PARTICLES AND OXIDIZED NANOASPERITIES

In the previous section, we have dealt with the Sb-HOPG incommensurable interface and have shown that, in accord with the previous theories, the incommensurability can account for the vanishing friction branch, see Fig 1. In this section, we provide simulation results for different single spacer particles and oxidized nanoasperities and show how they account for the other two frictional branches of Fig. 1. The picture emerging from these simulations is that spacer particles, while able to account for the normal friction branch, provide insufficient friction to account also for the after exposition to air branch. In order to account for the highest friction branch, we present in Sec. IV B a model based on mobile oxidized nanoasperities. Simulations in this section deal with each impurity considered separately. Simulations with multiple friction generators will be analyzed in Sec. V.

A. Spacer particles

In this section, we describe simulations of single, most common impurities in the Sb-HOPG interface associated with imperfect vacuum, namely, oxygen, water, hydrocarbons, and Sb_4 clusters. Oxygen is considered both in O_2 molecular as well as atomic states. Propane is chosen as a computationally feasible representative of hydrocarbons. Antimony clusters have been shown to grow from Sb_4 clusters.[23] Hence, we presume their presence on the HOPG substrate and consider also the smallest building unit of antimony as a spacer particle.

The oxygen molecule, O_2, is the most natural contaminant of the interface to consider. These simulations have been performed in spin-polarized spin-unrestricted mode. As shown in Fig. 5, the $^3\Sigma_g^-$ O_2 state of an isolated O_2 molecule is strongly modified by insertion into the Sb-HOPG interface. Insertion of the molecule into the interface is accompanied by charge transfer into the O_2 molecular orbitals. The two strongly antibonding pp $\pi^\star$ molecular orbitals are completely filled. As a result, the O_2 molecule dissociates. This is in stark contradiction with what happens if the O_2 molecule is adsorbed on the surface of the Sb or HOPG surface where the O_2 molecule remains intact.[24] From these results we conclude that due to the constraints exerted by the interface gap, the O_2 molecule is unstable in the interface and dissociates into atoms. The atoms from the dissociated O_2 molecules may follow different bonding patterns, which we follow below.

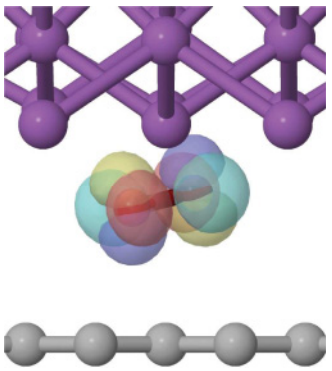

FIG. 5. (Color online) Electronic charge redistribution in the O_2 molecule upon insertion into the Sb-HOPG interface. Note the population of two strongly antibonding $\pi^\star$ molecular orbitals (yellow/light grey-blue/dark grey and green/light grey-red/dark grey).

One of the simplest models assuming the oxygen atoms incorporated in the Sb_n particle is shown in Fig. 6. While the oxygen minitips generate an appreciable corrugation of the PES of ≈65 meV, their rigidity, evidenced by the absence of any angular motion, Fig. 6, means that their effect on an incommensurable underlying substrate will cancel out. Hence, in addition to O_2 molecule also simply bonded single oxygen atoms can be ruled out as friction generators responsible for the two linear scaling frictional branches of Fig. 1.

Results for a single water molecule, shown in Fig. 7, indicate appreciable energy barriers of ≈100 meV. Monitoring of the motion pattern reveals that while water moves along with antimony, its angle with respect to HOPG, $\vec{AB}, \vec{cd}$, varies in a regular pattern corresponding to rotation of the molecule around the oxygen atom, see Fig. 7. As stressed in Sec. I, this molecular motion is of key importance for overcoming the averaging effect of the incommensurability of the sliding interface, see Fig. 2. Hence, the forces generated by individual dirt particles will not cancel out but rather sum up. A rough estimate of friction force generated by one H_2O molecule yields $F_1 = \frac{1.602 \times 100}{0.8} = 200$ pN. Hence, a dirt concentration from the measured forces on the normal branch of Fig. 1 yields

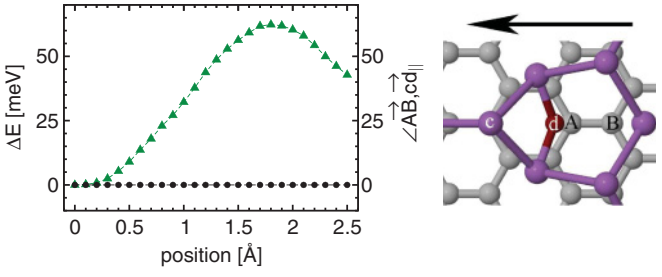

FIG. 6. (Color online) Oxygen atom incorporated into Sb-HOPG interface. Left panel: PES (green/grey triangles) and angles characterizing spacer particle motions (black dots) upon sliding the interface. Right panel: geometry of the interface (HOPG shown as small grey hexagons and antimony as large violet/dark grey hexagons) with an oxygen atom. Motion of the spacer atom is depicted by the $\vec{AB}, \vec{cd}_\parallel$ angle (in degrees) with $\parallel$ denoting projection into the HOPG plane. The upper arrow indicates the sliding direction of the interface.

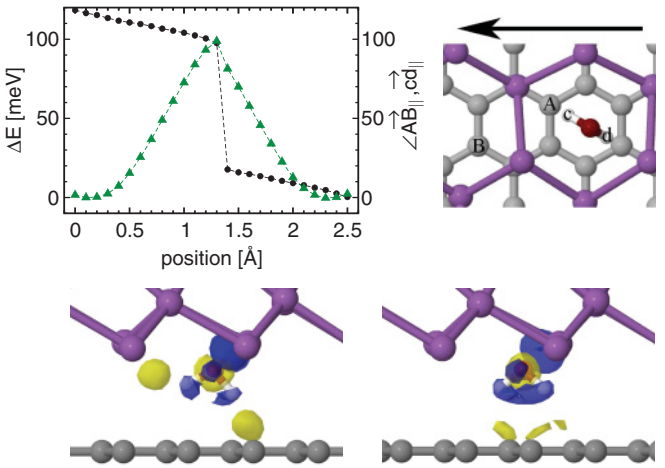

FIG. 7. (Color online) Water molecule incorporated into Sb-HOPG interface. Color/grey-scale coding of the PES and molecular mobility characterized by the $\vec{AB}, \vec{cd}$ angles as in Fig. 6. Bottom two panels show induced electronic charge upon insertion of water into the interface for geometries corresponding to minimum (left), and maximum energy (right). Yellow/light grey color corresponds to charge pile up, blue/dark grey color to charge depletion.

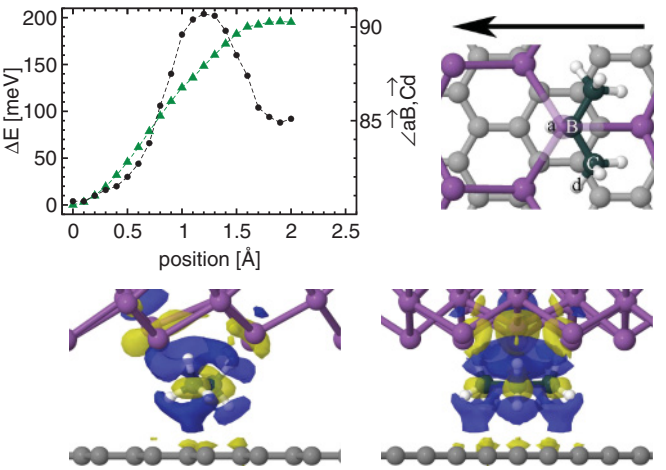

FIG. 8. (Color online) Propane spacer molecule incorporated into the Sb-HOPG interface. Color/grey-scale coding of the PES, molecular mobility, and charge densities as in Fig. 6. Bottom two panels show induced electronic charge upon insertion of propane into the interface. Red color corresponds to charge pile up, blue color to charge depletion. Left and right correspond to two different views of geometry corresponding to minimum energy.

$\frac{F_f/F_l}{A} \approx 1$ H_2O molecule/200 nm^2. This lower bound estimate appears reasonable and compatible with UHV conditions.

The molecular motions can be understood in terms of bonding to the interface shown in the bottom panels of Fig. 7, which depict charge densities induced by adsorption in the interface, i.e., $\Delta n(\vec{r})_{\mathrm{Sb-H_2O-HOPG}} - n(\vec{r})_{\mathrm{Sb-HOPG}} - n(\vec{r})_{\mathrm{H_2O}}$. Water molecule forms weak bonds to both antimony and HOPG around the minima of PES. Those bonds are broken as the molecule climbs the barrier. The bonds are reformed again after the molecule passes the maximum. The process of bond reforming is accompanied by a rapid molecular rotation.

Propane molecule was used as a representative of a hydrocarbon molecule. The results in Fig. 8 exhibit the largest corrugation of the PES of ≈200 meV among all molecules studied. A rough estimate of propane concentration from the measured force on the normal branch of Fig. 1 yields ≈1 propane molecule/400 nm^2, a reasonable lower bound estimate compatible with UHV conditions. The molecular motion is more involved in this case and can be described as motion of propane along with antimony surface with methyl groups rotating with respect to the methylene group.

Unlike water, the electronic response of the interface upon insertion of propane is more difficult to understand, see the bottom panels of Fig. 8. Propane is a closed-shell molecule whose insertion into the Sb-HOPG surface induces complicated charge transfers leading to electrostatic bonding of the molecule to the interface.

Results for Sb_4 spacer cluster shown in Fig. 9 indicate small energy barriers of ≈15 meV. Again, as in the case of water, analysis of the motion pattern reveals that Sb_4 moves along with antimony with its angle with respect to HOPG varying in a regular pattern, see Fig. 9. This motion represents essentially a rotation of the Sb_4 unit in order to position it in an energetically more favorable configuration with respect to HOPG around the maxima of the PES. A rough estimate of dirt concentrations from measured forces on the normal branch yields ≈1 Sb_4 particle/18 nm^2. This estimate may seem too large to be compatible with UHV conditions. However, the high concentration of Sb_4, if indeed present, may be understood as a consequence of the "roughness" of the Sb-HOPG interface.

This simulation result can be used to obtain another estimate of the frictional force for the incommensurable Sb-HOPG interface assuming amorphous structure. As an upper estimate we can use this result together with the square root scaling to predict a theoretical friction value of ≈3 nN for a 30×10^3 nm^2 particle consistent with the experimentally observed vanishing friction branch in Fig. 1.

B. Oxidized nanoasperities

Having provided insights into both vanishing and non-vanishing frictional branches, we now proceed to the exposed to ambient conditions branch, see Fig. 1. Can the other frictional duality arising after exposure to ambient conditions be explained purely by presence of a large number of dirt particles? Using the same molecules as in the case of the normal friction branch, we arrive at the lower bound concentration estimates of ≈1 H_2O molecule/20 nm^2,

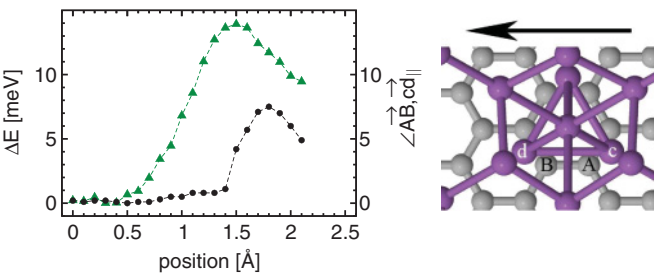

FIG. 9. (Color online) Sb_4 spacer cluster incorporated into the Sb-HOPG interface.

≈1 propane molecule/40 nm^2, and ≈1 Sb_4 particle/1.8 nm^2 for the after-exposure-to ambient-conditions branch. While estimates of contaminant concentrations under UHV conditions are not easy, all three concentrations appear much too high. More importantly, unlike the first frictional duality arising in UHV conditions, increased concentration of spacer particles can categorically be excluded as the cause for the following reason. Both superlubric and normal nanoparticles are equal, as initially superlubric particles may turn normal after contamination by spacer particles.[8] By exposure to ambient conditions all particles are initially contaminated, i.e., equal. Hence, sole contamination can only lead to a single frictional branch, as was the case in particles prepared in vacuum. Hence, the second duality must correspond to a completely different mechanism. The simplest model assuming the oxygen atoms incorporated in the Sb_n particle was analyzed above and excluded as a friction generator due to their rigidity and absence of any angular motion, see Fig. 6. A more plausible model is analyzed in the following in terms of a novel concept of oxidized mobile nanoasperities.

In accord with the above consideration of the presence of Sb_4 particles as one type of impurity in the Sb-HOPG interface studied above, we now consider oxidation of the Sb_4 nanoasperities to form Sb_4O_6-type minitips. Isolated Sb_4O_6 nanoparticles have been studied in the past and found to be stable.[25] Alternatively, Sb_4O_3 clusters could be considered as equally stable friction generators with very similar frictional properties. We note that the presence of Sb_4 in the interface is not strictly required, as Sb_4O_6/Sb_4O_3 minitips may also be formed by local oxidation of the Sb_n nanoparticles without the presence of Sb_4 precursors,[24] a scenario analyzed below. The results for Sb_4O_6 clusters, shown in Fig. 10, not only exhibit large PES corrugation of ≈130 meV but they also exhibit the mobility required in order to prevent the effect of formation of an incommensurable interface structure. The motion of the oxidized nanoparticle essentially corresponds to lateral displacements in order to avoid the energetically most unfavorable configurations. A lower bound estimate of concentration of the Sb_4O_6 nanoparticles based on a fit to the forces on the exposed-to-the-air branch yields a high value

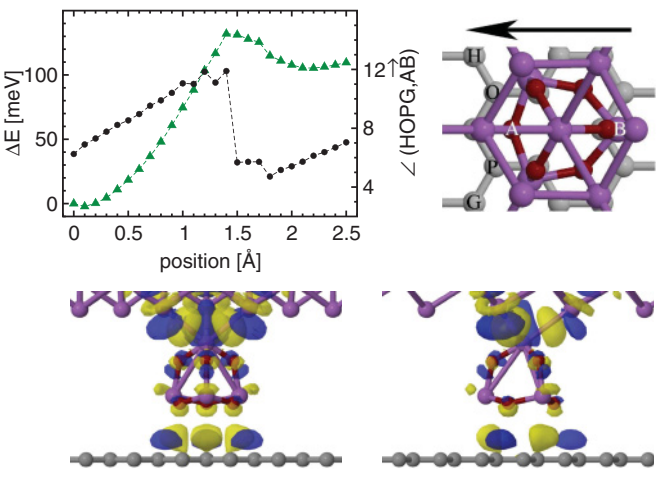

FIG. 10. (Color online) Sb_4O_6 spacer cluster incorporated into Sb-HOPG interface.

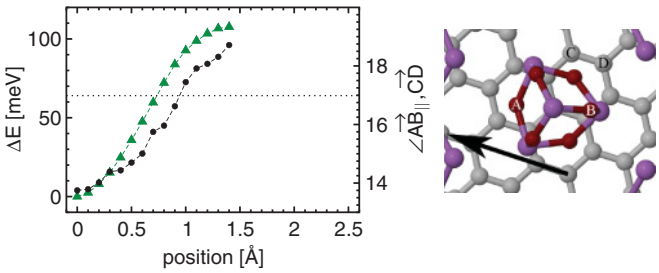

FIG. 11. (Color online) Sb_4O_6 spacer cluster formed by local oxidation of antimony surface incorporated into Sb-HOPG interface. Note that the Sb_4O_6 minitip is dug deeper in the surface. Horizontal line indicates rotation of the antimony cell with respect to HOPG.

of ≈1 Sb_4O_6/20 nm^2. However, this large concentration is fully compatible with UHV conditions, meaning essentially presence of fully oxidized nanocontacts after the air exposure.

As shown in the bottom panels of Fig. 10, bonding of Sb_4O_6 to Sb-HOPG interface is similar in nature to that of propane, i.e., electrostatic, albeit weaker, due to alternating positive and negative induced charges at the Sb_4O_6-HOPG interface.

An alternative to the above concept of oxidized Sb_4O_6 nanoasperities formed from Sb_4 precursor clusters is a concept of local oxidation of the antimony nanoparticle surface. Presence of oxygen in antimony leads to formation of Sb_4O_6/Sb_4O_3 type of minitips similar to those formed from the Sb_4 precursors. The propensity to local oxidation can easily be verified computationally, even though the energetics and thermodynamics of that process is far beyond the scope of this study. The main difference being that the minitips formed by local oxidation of antimony are inserted deeper into the antimony surface, see Fig. 11. This fact may limit the mobility of the minitip. We defer the study of the mobility to the next section. We note in passing that, given the high concentration of the oxidized minitips, the concept of local oxidation of antimony surface to form mobile Sb_4O_6/Sb_4O_3 nanoasperities is more likely than the scenario based on the presence of a high concentration of oxidized Sb_4 precursors.

The results for the local oxidation scenario are shown in Fig. 11. Due to the fact that these nanoasperities protrude deeper in the Sb surface, they create stress fields that the smaller model of the Sb-HOPG incommensurable interface cannot accommodate. For that reason a larger supercell had to be used, see Sec. III. Not surprisingly, the results in Fig. 11 resemble those for the oxidized Sb_4O_6 particles formed from Sb_4 precursors, yielding concentration of ≈1 Sb_4O_6/20 nm^2 based on the force fit on the exposed to the air branch.

V. MULTIPLE SPACER PARTICLES

So far we have considered various single contaminants and made upper/lower bound predictions of frictional forces/dirt concentrations based on their linear scaling with contact area.[11] From Fig. 2 it is intuitively clear that structure, morphology, and placement of dirt particles will play an important role in generation of frictional forces. We provide below a case study for two water molecules. A similar study was conducted also for two Sb_4 clusters with similar results. However, the maximum supercell size we can adopt in our simulations

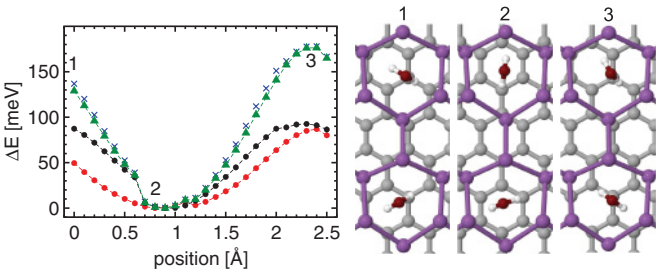

FIG. 12. (Color online) Two water molecules incorporated into Sb-HOPG interface at sites where an in-phase amplification of their effect is to be expected, see Fig 2. Left panel: PES for two H_2O spacers molecules (green/grey triangles), red/grey and black dots depict the PESs of the first and second water molecule considered separately. Blue/grey crosses show the exact sum of PESs of the two water molecules considered separately. Right panel: configurations sampled from the simulation at points 1, 2, and 3, shown in the left panel.

severely limits these results. Hence, we reveal here only simulations of two water molecules, two Sb_4O_6 asperities formed without Sb_4 precursors by a direct oxidation of the antimony surface, and a combination of Sb_4, water, and propane dirt particles.

A. Multiple water molecules

In order to verify the concept of mobile spacer molecules avoiding averaging out effects, see Fig. 2, we have placed two water molecules in an incommensurable Sb-HOPG interface. Two simulations have been performed. In the first, see Fig. 12, two molecules were positioned so as to emulate an in-phase summation, whereas in the other, see Fig. 13, an out-of-phase summation was emulated.

Results in Fig. 12 demonstrate unambiguously the presumed summation effect; both energies and forces double, compared to results for a single H_2O molecule in Fig. 7. The geometry in the center figure corresponds to a minimum with both H_2O molecules bridging a C_6 ring, whereas the maxima correspond to the two geometries to the left/right with both molecules straddling a C-C bond.

Results in Fig. 13 demonstrate absence of the averaging out effect. The results are in between complete averaging out and perfect summing, see Fig. 12, and correspond roughly to results of a single H_2O molecule, Fig. 7. The geometry in the center figure again corresponds to a minimum with both H_2O molecules bridging a C_6 ring. The maxima correspond to two geometries to the left/right with one molecule bridging a C_6 ring and one straddling a C-C bond. As can be seen in Fig. 13, a local minimum has formed around the position at 2 Å, where one H_2O molecule failed to relax completely. Such an effect will be strongly counteracted by thermal motions of the molecule at finite temperatures.

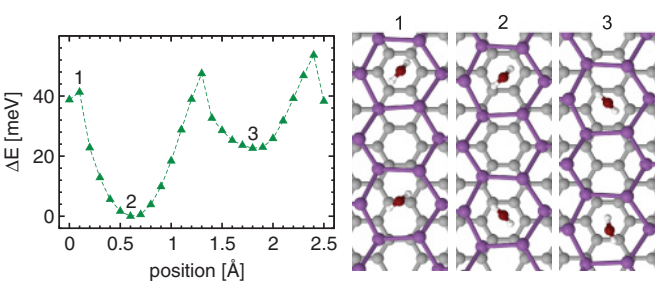

FIG. 13. (Color online) Two water molecules incorporated into Sb-HOPG interface at sites where an out-of-phase combination of their effect is to be expected, see Fig 2. Meaning of left and right panels as in Fig. 12.

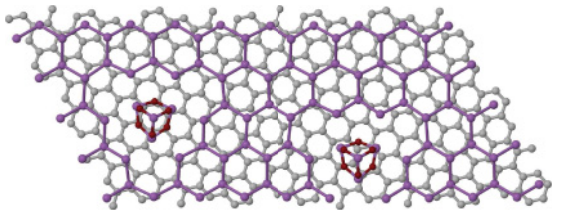

FIG. 14. (Color online) Two Sb_4O_6 spacer clusters corresponding to local oxidation of antimony surface incorporated into the Sb-HOPG interface at sites where an out-of-phase combination of their effects is to be expected, see Fig 2.

The combined effect of these and similar molecular motions will result in increase of frictional forces, which will scale linearly with contact area.

B. Multiple Sb_4O_6 spacer clusters formed by local oxidation of antimony

In this section, we test the mobility of multiple Sb_4O_6 minitips and the associated ability to avoid averaging-out effects of the frictional forces. Due to the fact that the minitips are dug deeper in the surface, less mobility can be expected with the result of more tendency toward averaging-out effects. To this end, we placed two Sb_4O_6 nanoasperities into the Sb-HOPG interface in positions where canceling of the PESs should be expected. However, in this case even the larger supercell, see Sec. III, turned out to be small. Hence, we have doubled the simulation cell size in one direction, see Fig. 14. The resulting system is too large for sliding simulations to be practical. For that reason we have only performed simulations for two different positions of the Sb-HOPG interface. We indeed found an energy difference of ≈104 meV, similar to that found for one particle, see Fig. 11, with typical rotations of 6° for left minitip. Hence, we conclude that the mobility is sufficient to prevent averaging out effects.

C. Combination of different spacer particles

Results in Fig. 15 demonstrate the effect of placing simultaneously into the Sb-HOPG interface all spacer molecules identified in Sec. IV A as efficient friction generators, i.e., water and propane molecules and Sb_4 cluster. The reason for placing different species simultaneously into the interface is to test their synergy in generating frictional forces. While the concentration of the spacer particles is unrealistically high, which may cause some artifacts, Fig. 15 clearly demonstrates that the cooperative effect in friction generation may be completely absent.

Initially there was a quick increase in the PES formation followed by a strong relaxation effect that occurred at position ≈3 Å in the simulation. The relaxation resulted in tipping over

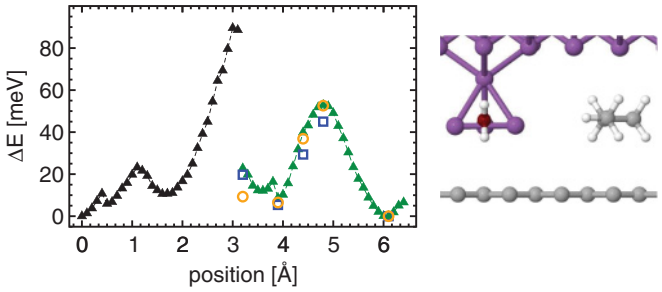

FIG. 15. (Color online) Sb_4, H_2O, and propane spacer particles simultaneously incorporated into the Sb-HOPG interface. Black and green/grey triangles: total corrugation of the PES before and after reconstruction of the spacer particles took place; orange/light grey circles: PES without water molecule; blue/dark grey squares: PES without propane molecule.

the Sb_4 cluster. Such a relaxation is very likely an artifact of high dirt concentration, as a similar relaxation was not observed in simulations with two Sb_4 clusters performed in a larger cell. Nevertheless, the analysis in Fig. 15 shows that all friction is completely determined by the flipped over Sb_4 cluster, with water and propane contributing nothing. In addition, one would intuitively predict that the friction force would be generated at the spacer particle-HOPG contact. However, analysis performed by removing the Sb_4 species indicates that ≈60% of the friction is not generated at the spacer particle-HOPG contact, but rather deeper inside the Sb nanoparticle as an effect of the stress generated by the Sb_4 particle.

This simulation shows clearly that the individual contributions of the different friction generators may not sum up as was the case for the multiple identical mobile friction generators studied above, see also Fig. 2.

VI. CONCLUSIONS

We have performed an extensive simulation study of frictional behavior of antimony nanoparticles on HOPG surface with the quest to shed light on the recent experiments.[7–9] Our simulations with aspirations clarify from first-principles simulations the behavior of a single asperity contact, and hence clarify the basic paradigm of nanotribology. The insights are supported by analyses of the bonding properties at the single asperity level.

By considering explicitly an incommensurable Sb-HOPG interface, a range of different mobile spacer molecules and clusters, and mobile oxidized nanoasperities, we have been able to shed light on the underlying physics and chemistry processes and provide qualitative explanation of all three frictional branches identified experimentally.[7–9] At the same time, quantitative upper/lower bound estimates of frictional forces/concentrations of mobile spacer particles could be provided. In addition, the simulations of single and multiple elementary friction generators provide the first insights into the molecular motions and atomistic reasons for avoidance of the averaging-out effects which would result froim rigid asperity contacts. Atomic/molecular-scale modeling of these aspects are beyond the capabilities of the existing theories,[10–14] which rather underline the genuine common nanotriboligical features. Most of the novel insights have been gained for the frictional branch corresponding to exposure to ambient conditions where the previous theories offer no explanation at all. Our concept of mobile oxidized nanoasperities along with the chemical insights provide a solid fundament for clarification of the high-frictional branches.

Beyond providing insights into one particular system, these simulations provide much wider appeal with many concepts being transferable to other systems. The parameters and computed PESs can be used in more coarse-grained modeling.[5] Yet, there are still nagging questions remaining. For example, why is it that the frictional branches are experimentally so clearly separated? We believe that one reason is that the Sb-HOPG is predominantly a vdW interface. If interfaces with more propensity to reconstruction and formation of stronger bonds were used, the clear separation between vanishing and nonvanishing branch is expected to disappear. On the other hand, the reason for a clear separation between the normal and after-exposition-to-air branches is more difficult to rationalize as it would require simulation of the thermodynamics and kinetics of the oxidation processes, which is clearly too difficult. More generally, more systematics should be brought into the field of nanotribology by systematic modifications of the nanoparticles as well as substrates. From the discussion above follows that in other related systems a different number of separate branches is to be expected. Research along those lines is now under way.[26]

ACKNOWLEDGMENTS

Financial support from APVT (ESF-EC-0007-07) under the Nanoparma ESF FANAS project is gratefully acknowledged. This research was supported in part by ERDF OP R&D, Project CE QUTE ITMS 26240120009, and via CE SAS QUTE (grants to J.B., R.T. and I.S.).

APPENDIX: MODEL TESTS

Here, we present a summary of part of the tests of the simulation model we have performed. We have considered HOPG, antimony crystal, and small Sb_n clusters. Geometries and energetics of all these systems were described with the usual DFT accuracy. Taking the structure of the Sb crystal as a typical example, we find for this, partially vdW bonded

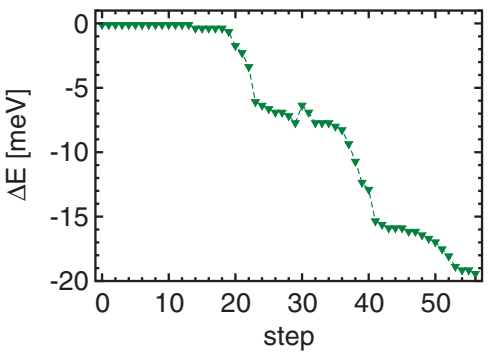

FIG. 16. (Color online) Total energy variation of Sb_4 cluster on HOPG determining the diffusion barrier as a function of the optimization step number.

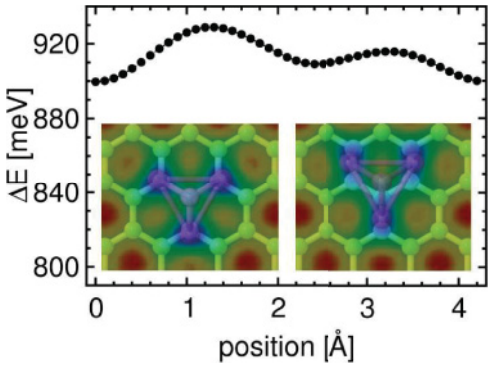

FIG. 17. (Color online) PES for sliding Sb_4 cluster on HOPG revealing the energy separation between vdW and chemical components; for details see the text. The insets show two configurations sampled from the simulation with electronic charge densities on the HOPG plane determining the chemical bonding element. The sliding direction is evident from the insets.

system, an agreement with the experimentally determined lattice constant to within 1.5%. This accuracy required a slight reparametrization of the Grimme's vdW correction term.[22]

In order to demonstrate the accuracy of description of the Sb-HOPG interface, we calculate the diffusion barrier of Sb_4 on HOPG, see Fig. 3. A rough estimate can be obtained from placement of Sb_4 at the transition state and allowing it to slide downhill on the PES, see Fig. 16. The diffusion barrier so determined yields $E_d > 20$ meV compared to experiments, which yield 40–60 meV.[23,27]

We have studied the details of the Sb-HOPG bond on a Sb_4-HOPG interface, see also Fig. 3. A clear separation between the vdW and "chemical" bonding components can clearly be distinguished. The vdW component provides most of the interaction energy between antimony and HOPG, but it provides very little corrugation of the PES for sliding and

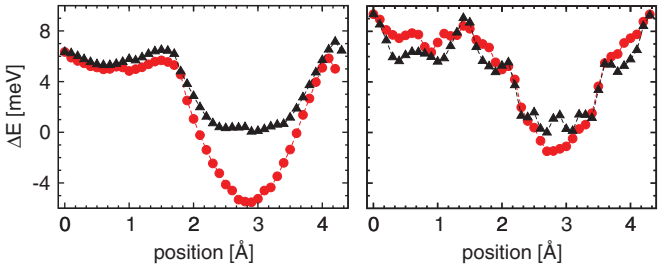

FIG. 18. (Color online) Variation of total energy as a function of the number of HOPG layers included in the simulation for Sb_4 cluster (left panel) and Sb_4O_6 oxidized asperity (right panel) sliding on HOPG substrate represented by a single layer (black triangles) and by four layers (red/grey circles).

hence, generates no friction. The situation is illustrated in Fig. 17. The vdW component accounts for ≈0.9 eV or ≈0.3 eV/atom, and the short-range chemical interaction accounts for corrugation of the PES of only ∼30 meV.

In production simulations, the HOPG surface in the "chemical region" was simplified and reduced to a single layer, see also Fig. 3. We have tested the effect of this approximation. In these tests we have selected a direction of a very low corrugation of the PES, which simultaneously maximizes the effect of the missing layers. The tests have been performed for Sb_4 and Sb_4O_6 clusters sliding over a single HOPG layer and over a HOPG slab formed by four layers. In all simulations, rotations of the clusters have been prevented. The results shown in Fig. 18 represent upper bound estimates of the error due to the use of a single HOPG layer. In the case of Sb_4 the error amounts to about ≈5 meV and ≈2 meV for Sb_4O_6. These errors are significantly smaller than the typical corrugations of the PESs (≈30 meV) and comparable to the accuracy of our simulations and, hence, are insignificant.

*ivan.stich@savba.sk

[1] *Nanotribology and Nanomechanics*, edited by B. Bushan (Springer, Berlin, 2005).
[2] B. N. J. Perssona, O. Albohrb, F. Mancosuc, V. Peveric, V. N. Samoilova, and I. M. Sivebaek, Wear **254**, 835 (2003).
[3] A. Schirmeisen and U. D. Schwarz, ChemPhysChem **10**, 2373 (2009).
[4] C. Ritter, M. Heyde, B. Stegemann, K. Rademann, and U. D. Schwarz, Phys. Rev. B **71**, 085405 (2005).
[5] I. Barel, M. Urbakh, L. Jansen, and A. Schirmeisen, Phys. Rev. Lett. **104**, 066104 (2010).
[6] L. Jansen, H. Hölscher, H. Fuchs, and A. Schirmeisen, Phys. Rev. Lett. **104**, 256101 (2010).
[7] D. Dietzel, C. Ritter, T. Mönninghoff, H. Fuchs, A. Schirmeisen, and U. D. Schwarz, Phys. Rev. Lett. **101**, 125505 (2008).
[8] D. Dietzel, T. Mönninghoff, C. Herding, M. Feldmann, H. Fuchs, B. Stegemann, C. Ritter, U. D. Schwarz, and A. Schirmeisen, Phys. Rev. B **82**, 035401 (2010).
[9] J. Brndiar, R. Turanský, D. Dietzel, A. Schirmeisen, I. Štich, Nanotechnology **22**, 085704 (2011).
[10] M. H. Müser, L. Wenning, and M. O. Robbins, Phys. Rev. Lett. **86**, 1295 (2001).
[11] G. He and M. O. Robbins, Phys. Rev. B **64**, 035413 (2001).
[12] M. Hirano and K. Shinjo, Phys. Rev. B **41**, 11837 (1990).
[13] M. H. Müser, Europhys. Lett. **66**, 97 (2004).
[14] G. He, M. H. Müser, and M. O. Robbins, Science **284**, 1650 (1999).
[15] J. Donohue, *The Structures of the Elements* (Wiley, New York, 1974).
[16] I. Štich, Acta Phys. Slov. **57**, 1 (2007).
[17] D. Marx and J. Hutter, in *Modern Methods and Algorithms of Quantum Chemistry*, edited by J. Grotendorst (NIC, FZ Jülich 2000), p. 301; for the code see [www.cpmd.org]. The CPMD subroutine evaluating vdW corrections had to be modified to accommodate surface geometries.
[18] J. P. Perdew, K. Burke, and M. Ernzerhof, Phys. Rev. Lett. **77**, 3865 (1996); **78**, 1396(E) (1997).
[19] Y. Zhang and W. Yang, Phys. Rev. Lett. **80**, 890 (1998).

[20]D. Vanderbilt, Phys. Rev. B **41**, 7892 (1990).
[21]G. B. Bachelet, D. R. Hamann, and M. Schluter, Phys. Rev. B **26**, 4199 (1982).
[22]S. Grimme, J. Comp. Chem. **27**, 1787 (2006).
[23]B. Stegemann, C. Ritter, B. Kaiser, and K. Rademann, J. Phys. Chem. B **108**, 14292 (2004).
[24]P. Ma and A. J. Slavin, Phys. Rev. B **49**, 8340 (1994).
[25]S. J. Gilliam, J. O. Jensen, A. Banerjee, D. Zeroka, S. J. Kirkby, and C. N. Merrow, Spectrochim. Acta, Part A **60**, 425 (2004).
[26]J. Brndiar, R. Turanský, and I. Štich (unpublished).
[27]Z. Yan, S. S. Kushvaha, W. Xiao, and X.-S. Wang, Appl. Phys. A **88**, 299 (2007).